Mon. Not. R. Astron. Soc. **359,** 1386–1392 (2005) doi:10.1111/j.1365-2966.2005.08994.x

Hyperfine splitting of [Al VI] 3.66 μm and the Al isotopic ratio in NGC 6302

S. Casassus,[1⋆] P. J. Storey,[2] M. J. Barlow[2] and P. F. Roche[3]

[1]*Departamento de Astronomía, Universidad de Chile, Casilla 36-D, Santiago, Chile*
[2]*Department of Physics and Astronomy, University College London, Gower Street, London WC1E 6BT*
[3]*Denys Wilkinson Building, Physics Department, Oxford University, Keble Road, Oxford OX1 3RH*

Accepted 2005 March 1. Received 2005 January 24; in original form 2004 October 14

ABSTRACT

The core of planetary nebula NGC 6302 is filled with high-excitation photoionized gas at low expansion velocities. It represents a unique astrophysical situation in which to search for hyperfine structure (HFS) in coronal emission lines from highly ionized species. HFS is otherwise blended by thermal or velocity broadening. Spectra containing [Al VI] 3.66 μm $^3P_2 \leftarrow {}^3P_1$, obtained with Phoenix on Gemini South at resolving powers of up to 75 000, resolve the line into five hyperfine components separated by 20–60 km s^{-1} as a result of the coupling of the $I = 5/2$ nuclear spin of ^{27}Al with the total electronic angular momentum J. The isotope ^{26}Al has a different nuclear spin of $I = 5$, and a different HFS, which allows us to place a 3σ upper limit on the ^{26}Al/^{27}Al abundance ratio of 1/33. We measure the HFS magnetic dipole coupling constants for [Al VI], and provide the first estimates of the electric quadrupole HFS coupling constants obtained through astronomical observations of an atomic transition.

Key words: atomic data – atomic processes – line: identification – line: profiles – ISM: abundances – planetary nebulae: individual: NGC 6302.

1 INTRODUCTION

The interaction between the electronic wavefunction and a non-zero nuclear magnetic dipole splits a fine-structure level $\{L, J\}$ into hyperfine levels. While hyperfine transitions are common in the radio range, at shorter wavelengths atomic hyperfine structure (HFS) has seldom been resolved in emission. Examples of hyperfine broadening include solar absorption lines from neutral species (Abt 1952), such as Mn I, whose transitions at 1.7743 μm are a rare example of unblended hyperfine lines (Meléndez 1999). Booth & Blackwell (1983, and references therein) summarize the effects of HFS on stellar spectra: its neglect results in incorrect measures of line broadening, and mismatched curves of growths, leading to ∼0.2 dex errors in the inferred photosphere elemental abundances, even for faint lines far from saturation. Both HFS and saturation lead to line broadening. This degeneracy complicates the use of stellar absorption lines as diagnostic of the hyperfine coupling constants. Hyperfine splitting can also be resolved in interstellar Na I D-line absorption in the local interstellar medium (ISM), which requires resolving powers of $\gtrsim 5 \times 10^5$ (Wayte, Wynne-Jones & Blades 1978; for more recent data, see Barlow et al. 1995).

The 1.8-MeV γ-ray emission due to the decay of ^{26}Al into ^{26}Mg has been the object of extensive space-borne surveys: with a half-life of 7.2×10^5 yr, ^{26}Al is a signpost of recent nucleosynthesis. Line emission at 1.8 MeV from the diffuse ISM (as observed by COMPTEL; Diehl et al. 1995) is consistent with a ^{26}Al source either in asymptotic giant branch (AGB) stars (Forestini, Arnould & Paulus 1991), novae, supernovae and Wolf-Rayet stars (Prantzos 2004) or from cosmic-ray collisions in molecular clouds (Clayton 1994). The *INTEGRAL* (Winkler et al. 2003) mission holds the promise of improved angular resolution with which to identify the most important contributor to the diffuse emission.

Although the decay of ^{26}Al is observed in the ISM at large, the ^{26}Al/^{27}Al isotopic abundance ratio (hereafter $R_{\rm iso}$) has never been measured in any astrophysical source. The only available upper limit in any specific object is that of Banerjee et al. (2004), who observed the vibronic bands of AlO at 1.5 μm in the nova-like variable V4332 Sgr, and reported an upper limit of ∼1/10, lacking a statistical discussion.

As an application of our detection of HFS in [Al VI] 3.66 μm $^3P_2 \leftarrow {}^3P_1$ (hereafter [Al VI]), which is the first in an astrophysical near-infrared emission line, we can set an upper limit on ^{26}Al/^{27}Al using the difference in the HFS of the two isotopes: the stable isotope ^{27}Al has a nuclear spin $I = 5/2$, while ^{26}Al has a nuclear spin $I = 5$. This new upper limit is the most stringent obtained so far in any astrophysical object.

The first detection of atomic HFS in emission, aside from the 21-cm H I line, is to our knowledge the observation of resolved HFS in [^{13}C II] 157.8 μm $^2P_{1/2} \leftarrow {}^2P_{3/2}$ by Boreiko, Betz & Zmuidzinas

⋆E-mail: simon@das.uchile.cl

Table 1. Observation log. The signal-to-noise ratio S/N is the ratio of the peak specific intensity to the noise in the image.

Date 2003	Slit (arcsec)	S/N	Integration (s)	Airmass	Seeing[a]	Weather[a]
May 07	0.25	14	84 × 180	1.27 → 1.03, 1.05 → 1.4	2	2
Jul 26	0.17	12	40 × 300	1.10 → 1.01 → 1.17	3	2
Jul 27	0.34	10	12 × 300	1.45 → 2.08	3	3
Jul 30	0.34	12	12 × 300	1.28 → 1.64	1	1
Jul 31	0.34	14	24 × 300	1.08 → 1.01 → 1.02	2	4

[a]Refer to a relative quality number, assigned by inspection, in which '1' is best.

(1988). Kelly & Lacy (1995) identified multiple components in [Na IV] 9.0 μm with the hyperfine splitting of $^3P_2 \leftarrow {}^3P_1$. Although [Na IV] 9.04 μm and [Al VI] 3.66 μm are the same fine-structure transitions from isoelectronic ions, they differ in nuclear spin and electronic wavefunctions, leading to different hyperfine structures.

We also derive values for the electric quadrupole constants (hereafter *B* constants) in the [Al VI] transition. To our knowledge, this is the first measurement of such constants in an atomic transition in any astrophysical object, although the *B* quadrupole constants have been measured in molecular transitions. In contrast with atomic HFS, in molecules the hyperfine splitting of a given rotational transition primarily derives from nuclear quadrupole moments rather than from nuclear magnetic moments (e.g. Townes & Schawlow 1955). For instance, *B* values have previously been measured by Turner & Gammon (1975) in CN($K = 1$–0) at 2.6 mm, and by Ziurys, Apponi & Yoder (1992) in $HCNH^+$($J = 1$–0) at 74 GHz. In this work we show that the inclusion of the atomic electric quadrupole terms has important spectroscopic consequences. It allows improved measurement of the magnetic dipole coupling constants by lifting the statistical bias between the magnetic dipole constants of the upper and lower levels.

In this work we demonstrate the use of HFS itself as a diagnostic tool in the context of planetary nebulae (PNe). Atomic hyperfine effects have previously been used by Clegg et al. (1997) in C III] λ1909.6 $^1S_0 \leftarrow {}^3P_0$ to measure the $^{13}C/^{12}C$ ratio in PNe. They recognized that the non-zero nuclear spin of ^{13}C additionally[1] mixes the $^3P_0$ and $^3P_1$ fine-structure states. C III] λ1909.6 is dipolar electric in ^{13}C, while it is completely forbidden in ^{12}C because it has no net nuclear spin. This C III multiplet is thus composed of three lines, one of which is due solely to ^{13}C.

NGC 6302 is the highest excitation PN known, with a spectrum rich in molecular lines, dust and coronal ions such as [Si IX] 3.93 μm, which can only be produced by photons harder than 303 eV, or by electron collisions at $T_e \approx 10^6$ K. Its spectrum can be reproduced by ionization-bounded photoionization models with a $T = 250\,000$ K central star (Casassus, Roche & Barlow 2000), and the absence of a fast wind makes a significant contribution from shock excitation improbable. Although the report of Meaburn & Walsh (1980) for broad wings under [Ne V] 3426 Å has been taken as evidence for a fast wind in NGC 6302, a 3000–10 000 Å echellogram we acquired with the Ultraviolet Echelle Spectrograph (UVES) on the Very Large Telescope (VLT) (Casassus et al., in preparation) does not confirm the observations of Meaburn & Walsh (1980). The photoionized coronal lines in NGC 6302 are astonishingly narrow (Ashley & Hyland 1988) compared to conditions of collisional ionization where their abundance is maximum. The linewidths measured by Casassus et al. (2000) reflect negligible thermal broadening from photoionized gas temperatures of 20 000 K, and very small expansion velocities in a filled-in nebula.

It is its small expansion velocity and rich spectrum that make NGC 6302 an ideal object for the use of hyperfine structure as a diagnostic tool.

We describe data acquisition in Section 2, then data analysis and results in Section 3, and summarize our conclusions in Section 4. Data reduction and analysis were carried out using the Perl Data Language.[2]

2 OBSERVATIONS

We observed NGC 6302 with Phoenix (Hinkle et al. 2003) on Gemini South on five nights of 2003 May and July, as summarized in Table 1. The slit position angle was 70° east of north, and it was centred on NGC 6302's radio core at J2000 RA = $17^h13^m44\overset{s}{.}4$, Dec. = $-37°06'11\overset{''}{.}2$, as inferred from the 5-GHz map of Gomez et al. (1989), at the position of the intensity decrease in the centre of the putative radio torus. Fig. 1 shows the slit position overlaid on the *R*-band image obtained with Gemini's acquisition camera. Background cancellation was obtained by differentiation with a reference field devoid of nebular emission, offset 40-arcsec north of the nebular core. Typical integration times in the [Al VI] settings were 1–2 h on-source for each night, but the noise level largely reflects the weather conditions. Poor weather also results in inaccurate background cancellation. The seeing has a direct impact on the resolution of the spectra, by convolving the emission in the slit with neighbouring emission from the expanding nebula. The emission that falls through the slit is the convolution of the slit aperture with the point spread function. Because of the spatial variations of radial velocity within the nebula, poor seeing allows emission from material with a wider range of velocities to be admitted by the spectrograph slit. The resulting spectra are therefore degraded by a combination of the instrumental resolution and the spatial variations in velocity.

The acquisition of a precise position in the nebula is important to obtain consistent spectra. To centre the slit on the position of the radio core of NGC 6302, we peaked-up on a reference astrometric standard in the *K* band, then offset to the object, switched detector settings and applied an additional offset to account for the difference in refraction between the filters. Peaking-up with a narrow slit is difficult because of variations in the seeing on time-scales comparable to the acquisition procedure. The accuracy involved in peaking-up depends on the seeing and the slit width. The overall positional

[1] This multiplet arises from the mixing of ^3P and ^1P states due to magnetic interactions between the electrons.

[2] http://pdl.perl.org

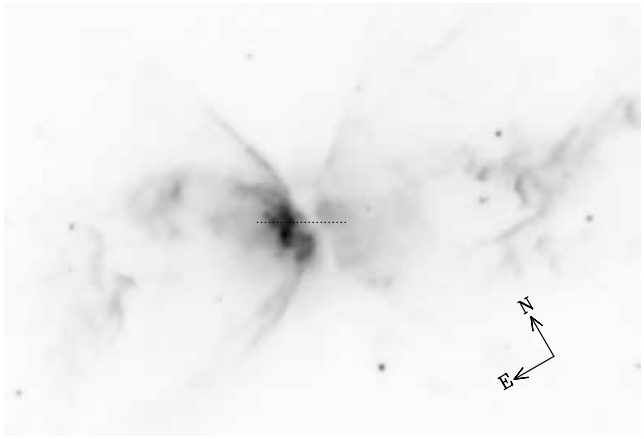

Figure 1. Overlay of the Phoenix 14 arcsec slit on the *R*-band Gemini acquisition image.

uncertainty is ∼0.6 arcsec, as estimated by adding in quadrature the errors involved in peaking-up, of about 0.35 arcsec (or twice the slit width), in offsetting from the reference star, of ∼0.5 arcsec, and in the filter change, of ∼0.1 arcsec (B. Rodgers, private communication).

The resulting spectra for the three best nights are shown in Fig. 2, after subtraction of a small level of continuum nebular emission. Wavelengths are given in air and in the observatory rest frame.

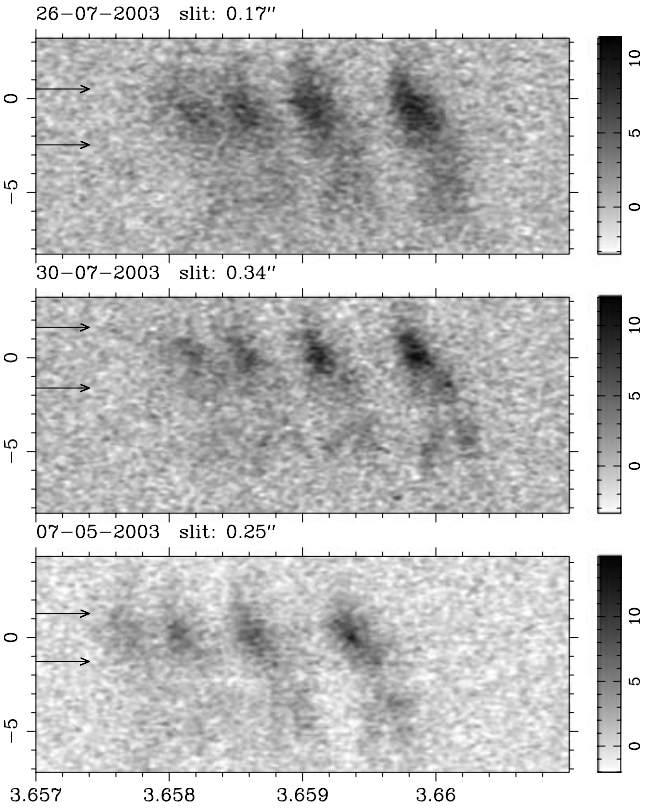

Figure 2. Phoenix detector array after flat-fielding, correcting for the slit tilt, and background and nebular continuum removal. Intensity is given in units of the noise on a linear grey-scale covering the full range of intensities. The *x*-axis is wavelength in μm; the *y*-axis is offset along the slit in arcsec, which increases towards the east. The horizontal arrows limit the optimal extraction aperture.

There are at least four emission features observed near the [Al VI] wavelength given by Casassus et al. (2000) of 3.659 μm. The three brightest features share similar position–velocity structures.

Because the 1-arcsec uncertainty in acquisition is larger than the slit width, spectra taken on different nights may not sample the same region in the nebula, so we only co-added the frames taken with the same instrumental setting (i.e. within the same night). Another reason to avoid averaging all the spectra is to keep a good spectral resolution: it can be inferred by inspection of Fig. 2 that the night of July 30 has the best line contrast, even though we used the widest slit. The sharpest lines should be obtained with the narrowest slit. The quality of the spectrum from July 30 reflects that it was acquired under the best weather conditions.

No reference lines were visible in the calibration exposures taken with a Th–Ar–Ne arc lamp in the [Al VI] instrument configuration. Instead, we used emission lines from co-added sky spectra extracted from the science observations (without differencing the nodded frames). We fit a straight line to the position of sky emission features present in a model high-resolution sky spectrum based on the HITRAN data base (Rothman et al. 1992). The accuracy of the inferred dispersion law is checked a posteriori by comparing different nights and previous wavelength measurements. The raw spectra are modulated by the atmospheric transmission (AT) spectrum, which is reasonably smooth near [Al VI] (AT does not show deep troughs). We correct for the AT modulation by dividing the object frames by the spectrum of a standard star (HR 6789) grown along the slit.

The optimal aperture for spectrum extraction in the spatial direction along the slit was determined by varying the upper $y_{\rm up}$ and lower $y_{\rm lo}$ rows of detector pixels. We summed all the signal in the detector within the rows $y_{\rm lo}$ and $y_{\rm up}$, and estimate the noise level a posteriori, from the rms dispersion of the output spectrum in a region devoid of line emission. A search in the 2D parameter space $\{y_{\rm lo}, y_{\rm up}\}$ for the spectrum with the best signal-to-noise ratio gives the optimal aperture indicated in Fig. 2. We hereafter refer to spectra extracted with this optimal aperture as 'collapsed spectra'.

3 HYPERFINE SPECTRAL FITS

In Russell–Saunders coupling the magnetic field due to the nuclear spin splits a given $\{L, J\}$ fine-structure level into hyperfine levels, with the following energy shifts (Glass & Hibbert 1978):

$$\Delta E(L, J, F, I) = \tfrac{1}{2}hA_{L,J}K + hB_{L,J}\left[K(K+1) - \tfrac{4}{3}I(I+1)J(J+1)\right], \quad (1)$$

where

$$K = F(F+1) - I(I+1) - J(J+1), \quad (2)$$

L stands for the electronic orbital angular momentum, I is the nuclear spin, h is the Planck constant, $A_{L,J}$ and $B_{L,J}$ are the magnetic dipole and electric quadrupole hyperfine coupling constants, respectively, and $F(F+1)$ is an eigenvalue of $\boldsymbol{F}^2$, where $\boldsymbol{F}$ is the vectorial $\boldsymbol{I} + \boldsymbol{J}$ operator. The relative intensities $S(\{J_1, F_1\}, \{J_2, F_2\})$ of each hyperfine component $\{I, J_1, F_1\} \leftarrow \{I, J_2, F_2\}$ can be derived from

$$S(\{I, J_1, F_1\}, \{I, J_2, F_2\}) = (2F_1+1)(2F_2+1)\begin{Bmatrix} F_2 & F_1 & 1 \\ J_1 & J_2 & I \end{Bmatrix}^2, \quad (3)$$

with the selection rule

$$|F_1 - F_2| \leqslant 1 \leqslant F_1 + F_2, \quad (4)$$

Table 2. The SUPERSTRUCTURE ab initio calculation of velocity shifts relative to the strongest component of ^{27}Al, and corresponding relative intensities, for [^{26}Al VI] and [^{27}Al VI].

^{27}Al VI		^{26}Al VI	
Rel. vel. (km s^{-1})	Rel. int.[a]	Rel. vel. (km s^{-1})	Rel. int.[a]
0.0	5.0 (1)	−14.8	9.0 (1)
−58.0	4.0 (2)	−49.5	7.8 (2)
−103.1	3.0 (3)	−79.3	6.6 (3)
−135.2	2.0 (2)	−104.1	5.4 (2)
−154.5	1.0 (1)	−107.3	4.2 (1)

[a]The number of subcomponents blended together in each velocity component is shown in brackets.

where $\{\}$ is the six-j symbol defined by Brink & Satchler (1994).

The model hyperfine structure of [Al VI] given in Table 2 derives from an ab initio calculation of the HFS coupling constants (carried out by one of us, PJS) using the atomic structure code SUPERSTRUCTURE (Eissner, Jones & Nussbaumer 1974; Clegg et al. 1997):

$$A^{\rm th}_{J=1}(^{27}{\rm Al}) = 0.2,\ A^{\rm th}_{J=2}(^{27}{\rm Al}) = 3461.8,$$
$$A^{\rm th}_{J=1}(^{26}{\rm Al}) = 0,\quad A^{\rm th}_{J=2}(^{26}{\rm Al}) = 1333, \tag{5}$$

where all values are given in MHz. Table 2 does not include the electric quadrupole terms in the hyperfine energy shifts, because SUPERSTRUCTURE does not currently predict the electric quadrupole hyperfine coupling constants. The velocities in Table 2 are all given relative to the strongest component of the stable isotope. The nuclear magnetic dipole moments used in the calculation are +3.64151 $\mu_{\rm N}$ for ^{27}Al (Raghavan 1989), and +2.804 $\mu_{\rm N}$ for ^{26}Al (Cooper et al. 1996), in units of the nuclear magneton $\mu_{\rm N} = e\hbar/2m_{\rm p}c$.

The hyperfine coupling constants given above were calculated in a simple two-configuration atomic model, $2s^22p^4$ and $2p^6$. Calculations were also made for more elaborate configuration bases and with different orbital optimization procedures, leading to a range of values for the hyperfine coupling constants. The results were all within 100 MHz of the values quoted above but with no obvious convergence to one particular best result. We therefore quote the results of the simplest calculation and adopt $\sigma^{\rm th} = 100$ MHz as the likely uncertainty in the theoretical result. This uncertainty has to be compared to the difference $|A^{\rm th}_{J=1} - A^{\rm th}_{J=2}| \sim 1000$, which is roughly how these quantities enter the expression for the hyperfine energy shifts. The theoretical $A^{\rm th}$ agree with observations within $2\,\sigma^{\rm th}$ (see below). The high accuracy of the calculation for ^{27}Al should be carried over to ^{26}Al since they have the same electronic wavefunctions (to a very good approximation). Therefore it is reasonable, within a <10 per cent uncertainty on the HFS coupling constants, to use the theoretical hyperfine constants for ^{26}Al in a fitting procedure to look for evidence of ^{26}Al.

There is no allowance for isotopic mass shift either in the ab initio calculations or in the spectral fits. We assume both ^{26}Al and ^{27}Al share the same line centroid. The normal mass shift (NMS) due to the difference in Rydberg constants between ^{26}Al and ^{27}Al would cause the centroid of the 3.6 μm line in ^{26}Al to be shifted to the red by 0.23 km s^{-1} relative to ^{27}Al. The specific mass shift (SMS) is not known for [Al VI] but measurements have been made for the same transition in the isoelectronic O I (De Natale et al. 1993), which show that the ratio of the total isotope shift to the normal mass shift, (NMS + SMS)/NMS, is 1.40 between ^{17}O and ^{16}O and 1.26 between ^{18}O and ^{17}O. Adopting the larger of these two values, we can estimate that the total isotope shift of the ^{26}Al centroid relative to ^{27}Al should be no more than 0.32 km s^{-1}.

For both isotopes there are actually nine lines, which in practice reduce to five due to degeneracy in the hyperfine levels associated with the $J = 1$ state. This degeneracy is not exact, but in practice the lines lie within less than 0.1 km s^{-1} of each other, which is much smaller than the typical linewidth of $\sigma \sim 8$ km s^{-1}, so they can be taken to have the same velocity shift. The number of components within each line is given in brackets in Table 2. We stress that Table 2 does not include the electric quadrupole terms in the hyperfine energy shifts.

We fit the [Al VI] line profile F_λ with the following parametrized model:

$$F_\lambda = F_0 + \sum_{i=1}^{N_{\rm isotope}} \sum_{g=1}^{N_{\rm gauss}} \sum_{F_1,F_2} S(\{I, J_1, F_1\}, \{I, J_2, F_2\}) \times R_i R_g \exp\left[-\frac{1}{2}\frac{[\lambda - \lambda_g(F_1, F_2)]^2}{\sigma_g}\right], \tag{6}$$

where F_0 is a constant baseline, $N_{\rm isotope}$ is the number of isotopes (i.e. one or two in this case), $N_{\rm gauss}$ is the number of Gaussians used to represent the fit (one or two), R_i is an overall amplitude for isotope i, and R_g is the relative amplitude of additional Gaussians relative to the first. Thus the first Gaussian component for isotope i has $R_{g=1} = 1$, and R_i is constant for all g components of isotope i. Finally, $\lambda_g(F_1, F_2)$ is the Gaussian centroid of each hyperfine component,

$$\lambda_g(F_1, F_2) = \lambda_0 + \Delta\lambda_g + \frac{ch}{\Delta E(L, J_2, F_2, I) - \Delta E(L, J_1, F_1, I)}, \tag{7}$$

where λ_0 is a reference wavelength that does not necessarily match the fine-structure transition, which instead corresponds to the overall centroid of the line, i.e. the average of each HFS component weighted by its flux, and $\Delta\lambda_g$ is an offset to describe the velocity profile with Gaussian g (one Gaussian has $\Delta\lambda = 0$).

The optimization was carried out by minimizing $\chi^2 = \sum_j [F(\lambda_j) - F_m(\lambda_j)]^2/\sigma_F^2$ in two steps. We perform an initial heuristic search of the global minimum with the PIKAIA genetic algorithm of Charbonneau (1995), and then optimize with the variable-metric routine MIGRAD of the MINUIT package from CERN (1998). We took the precaution of cross-checking the MIGRAD results with the downhill simplex method AMOEBA (Press et al. 1986), which we observe to be much slower and far less robust than MIGRAD (AMOEBA requires fine tuning of the input simplex and tolerance parameters). Errors on individual parameters are estimated by searching parameter space for the $\Delta\chi^2 = 1$ contour.

The resulting observed spectrum and model line profile are shown on Fig. 3. We show the case of the optimal extraction spectrum from July 30 in Fig. 3(a), together with an indication of the hyperfine splitting of ^{26}Al, had it been present. The co-added spectrum is compared to the fits in Fig. 3(b), where it can be appreciated that the inclusion of the electric quadrupole hyperfine terms improves the fit. It can be verified by inspection that the solid line, with B terms, is appreciably closer to the data than the dotted line, without B terms. The residuals are shown on Fig. 3(c), with the formal ^{26}Al fit.

Our best-fitting line profiles are summarized in Table 3. The ^{26}Al hyperfine coupling constants were kept fixed at their theoretical values, as specified in equations (5). We list reduced χ^2 as an indicator of goodness of fit: values much less than unity reveal that we are fitting the noise with an excessive number of free parameters. None

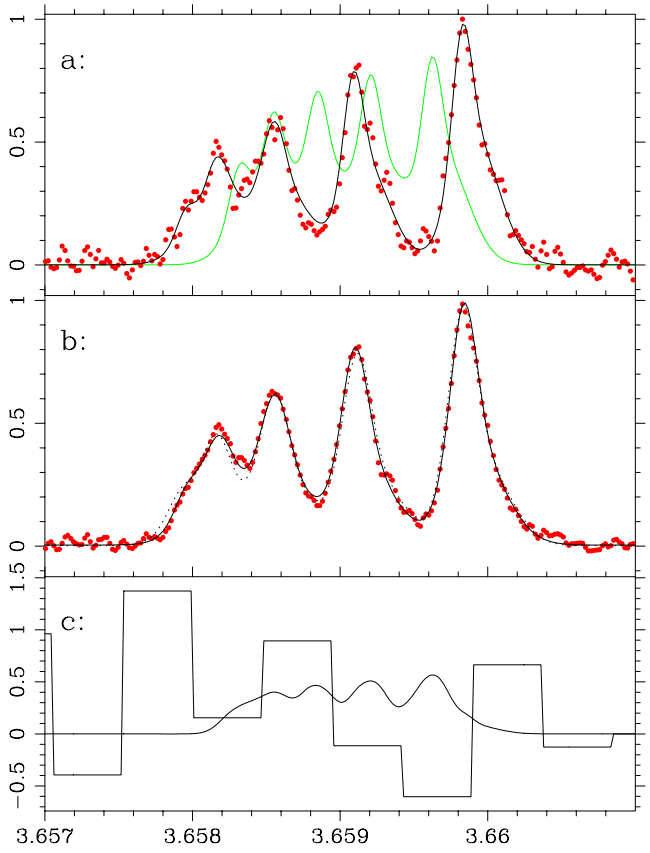

Figure 3. (a) Points: collapsed spectrum of [Al VI] from 2003 July 30, with the optimal extraction aperture. Solid line: the best fit with two Gaussians per component, and the parameters given in Table 3, without a contribution from ^{26}Al. Grey solid line: the profile of ^{26}Al, had it been present at a level giving an isotope ratio of unity. (b) Points: co-added spectrum. Solid line: combined model. Dotted line: combined model without electric quadrupole hyperfine splitting. (c) Histogram: binned residuals, excluding the ^{26}Al fits. Solid line: combined ^{26}Al fit.

the less we include these fits in the list with the goal of combining the results from all nights.

We can use the information that the HFS coupling constants are the same on each night to perform a second run of the fitting procedure, and fix the HFS constants to the average given in Table 3. This allows improved estimates of the fine-structure centroid, as well as tighter limits on the abundance of ^{26}Al relative to ^{27}Al. The results of this second run of fits are summarized in Table 4. The average value for the fine-structure centroid includes a correction for the heliocentric systemic velocity of NGC 6302 of -35.0 km s^{-1} (Casassus et al. 2000), and is accurate to within 1 km s^{-1}. The constraints we can place on the Al isotope ratio are summarized under the second and third columns. The 1σ values and upper limits indicated in column 2 are formal indicators of the relative limits set by each spectrum, and are derived from the first fitting procedure, with free HFS constants. In this case we cannot use the error estimates derived from the $\Delta\chi^2 = 1$ contour because the positivity requisite on $R_{\rm iso}$ precludes reaching the global χ^2 minimum with certainty. However, we relaxed the positivity constraint in the second fit, fixing the HFS constants. The results are listed in the third column. The weighted average for $100 \times R_{\rm iso}$ is 0.6 ± 0.8.

We estimate an upper limit on $R_{\rm iso}$ by generating a synthetic spectrum with $R_{\rm iso} = 0.03$, and repeating the fitting procedure, for 100 different realizations of Gaussian noise, at the same level as that of the collapsed spectrum for 2003 July 30 (which has the best S/N). This Monte Carlo error analysis shows that we can recover the input isotope ratio at 2σ: $100 \times R_{\rm iso} = 3.1 \pm 1.6$. Another simulation with the noise level of the residual spectrum shown on Fig. 3 gives $100 \times R_{\rm iso} = 3.0 \pm 0.8$. These simulations and the combined measurement of $R_{\rm iso}$ from Table 4 are in agreement, which allows us to place the following 3σ upper limit:

Table 4. The fine-structure centroid and limits on the Al isotope ratio.

Date 2003	$100 \times R_{\rm iso}$ Formal[a]	Best fit[b]	Wavelength[c] $\lambda_{\rm FS}$
May 07[d]	1.5 ± 2.5	4.8 ± 2.0	3.659273(35)
Jul 26[d]	<0.67	-0.4 ± 2.0	3.659427(19)
Jul 27[d]	1.8 ± 2.6	-1.5 ± 2.3	3.659415(22)
Jul 30[e]	1.6 ± 2.5	2.9 ± 2.3	3.659392(22)
Jul 30[d]	<0.88	-0.9 ± 1.7	3.659410(10)
Jul 31[d]	<0.72	-1.2 ± 2.2	3.659427(40)
Average	–	0.6 ± 0.8	3.659405(7)

[a]Formal 1σ upper limit (see text for accurate upper limits). [b]Best-fitting isotopic ratio, using fixed HFS constants. [c]Rest wavelength in μm and in air. [d]Collapsed slit (optimal S/N). [e]Six-row spectrum centred on the peak of emission.

Table 3. HFS fits to the observations for ^{27}Al.

Date 2003	Noise[a]	χ^2/ν	λ_0[b] (μm)	$A_{L,J=1}$[c] (MHz)	$A_{L,J=2}$ (MHz)	$B_{L,J=1}$ (MHz)	$B_{L,J=2}$ (MHz)	FWHM$_1$ (km s^{-1})	$\Delta\lambda_1$ (10^{-5} μm)	R_2	FWHM$_2$ (km s^{-1})
May 07[d]	4.4×10^{-2}	1.02	3.658715^{+35}_{-22}	-0.1^{+162}_{-153}	3489.1^{+79}_{-82}	-0.0^{+13}_{-13}	6.9^{+2}_{-2}	$18.3^{+1.0}_{-0.9}$	-15.1	0.56	$36.7^{+2.0}_{-2.7}$
Jul 26[d]	4.5×10^{-2}	0.98	3.659112^{+27}_{-27}	0.0^{+243}_{-231}	3499.1^{+117}_{-122}	0.0^{+22}_{-21}	10.5^{+4}_{-4}	$23.9^{+0.8}_{-0.9}$	-5.4	0.20	$65.2^{+11.6}_{-10.7}$
Jul 27[d]	7.0×10^{-2}	0.87	3.659341^{+9}_{-11}	417.7^{+123}_{-121}	3332.9^{+65}_{-66}	-54.6^{+11}_{-10}	16.9^{+2}_{-2}	$22.3^{+0.7}_{-0.7}$	-30.3	0.26	$11.6^{+2.2}_{-1.6}$
Jul 30[e]	6.3×10^{-2}	0.80	3.659247^{+16}_{-23}	258.2^{+150}_{-249}	3390.2^{+124}_{-76}	-19.7^{+15}_{-18}	8.7^{+3}_{-3}	$15.9^{+0.7}_{-0.8}$	-18.8	0.13	$8.8^{+3.8}_{-2.5}$
Jul 30[d]	4.1×10^{-2}	1.08	3.659125^{+13}_{-11}	276.9^{+98}_{-108}	3399.2^{+55}_{-50}	-29.8^{+8}_{-9}	9.3^{+2}_{-2}	$13.1^{+0.8}_{-0.8}$	-9.9	0.82	$31.4^{+0.9}_{-0.8}$
Jul 31[d]	5.3×10^{-2}	0.68	3.659365^{+32}_{-58}	-117.0^{+446}_{-238}	3575.9^{+122}_{-224}	-17.2^{+50}_{-17}	8.8^{+3}_{-9}	$17.1^{+0.6}_{-0.7}$	-30.2	0.11	$26.7^{+8.9}_{-6.1}$
Average				235.5 ± 62.8	3410.1 ± 32.4	-28.0 ± 5.3	10.7 ± 1.0				

[a]Noise used to assess the significance of the fits, normalized to the peak flux density (i.e. S/N = 1/noise). [b]Uncertainties on λ_0 refer to the last decimal places; λ_0 does not match the fine-structure centroid (see text and equation 7). [c]Uncertainties on all quantities refer to the usual 68.3 per cent confidence interval (i.e. 1σ for one parameter). [d]Collapsed slit (optimal S/N). [e]Six-row spectrum centred on the peak of emission.

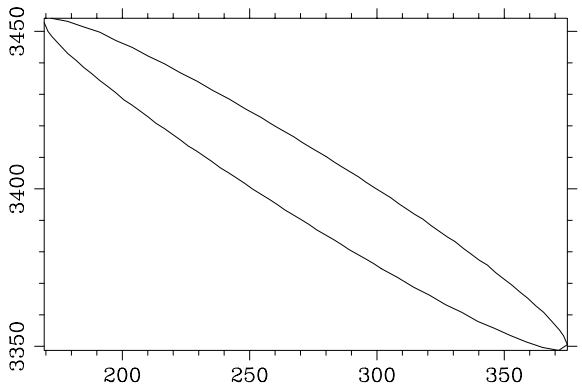

Figure 4. Bias due to the correlation of the free parameters for the HFS constants $A_{J=2}(^{27}\mathrm{Al})$ (y-axis) and $A_{J=1}(^{27}\mathrm{Al})$ (x-axis), from the collapsed spectrum of 2003 July 30.

$$R_{\rm iso} < \langle R_{\rm iso}\rangle + 3\sigma = 3.0 \times 10^{-2}. \quad (8)$$

The uncertainty in the measured HFS coupling constants, relative to the optimal value, is rather large compared to that of the central wavelengths. This is due to a significant statistical bias in the values of $A_{J=2}(^{27}\mathrm{Al})$ and $A_{J=1}(^{27}\mathrm{Al})$. Fig. 4 is a 2D slice in parameter space showing the correlation of both constants. With the neglect of the quadrupole HFS constants $B_{L,J}$, the bias is much stronger and the uncertainty on the magnetic dipole constants is much larger (∼5 times larger): $A_{J=1}(^{27}\mathrm{Al}) = 149^{+171}_{-444}$, $A_{J=2}(^{27}\mathrm{Al}) = 3499^{+224}_{-87}$. In the absence of the electric quadrupole terms, the hyperfine energy shifts depend on the $A_{L,J}$ constants approximately through their difference, $A_{J=2}(^{27}\mathrm{Al}) - A_{J=1}(^{27}\mathrm{Al})$. Notwithstanding this difficulty, the observed constants are close to the theoretical values used to produce Table 2.

The reasons why we are confident in our detection of the electric quadrupole hyperfine splitting are as follows.

(i) The fit to the line profile significantly improves, with reduced χ^2 increasing by more than 0.1 without the $B_J(^{27}\mathrm{Al})$ constants, systematically for all nights. For example, in the case of the collapsed spectrum for July 30, χ^2/ν rises from 1.08 to 1.20.

(ii) The improvement in the fit is visible to the eye by inspection of Fig. 3, where it can be appreciated that the fit without $B_J(^{27}\mathrm{Al})$ gives an excess in the blue.

(iii) The two electric quadrupole constants are measured with accuracies of 6σ and 10σ.

(iv) The average isotope ratio without the quadrupole terms is $(-1.41 \pm 0.59) \times 10^{-2}$, which reflects a tendency to compensate for the misfit with a negative, and spurious, amplitude for the rare isotope.

The intrinsic profile of [Al VI] is manifestly very narrow. A single Gaussian fit to the spectrum from 2003 July 30, with a six-row extraction centred on the peak of emission along the slit, gives a width of $\sigma = 7.31 \pm 0.24$ km s^{-1}, or a full width at half-maximum (FWHM) of 17.21 ± 0.56 km s^{-1}. This spectrum was acquired with the widest slit, and a resolving power $R = 40\,000$. We cannot give a precise measure of the instrumental resolution because of the lack of arc lines near [Al VI]. However, assuming $3 \times 10^5/R$ km s^{-1} corresponds to the FWHM instrumental resolution within 20 per cent, we can give an estimate of the deconvolved linewidth of 15.5 ± 1.0 km s^{-1} FWHM. A comparison with emission lines from lighter species is deferred to a forthcoming article.

4 CONCLUSIONS

We have identified the multiple components near [Al VI] as due to the HFS splitting of ^{27}Al. Theory agrees with the observed magnetic dipole HFS coupling constants within the uncertainties, giving support for the use of theoretical constants in the modelling of ionic lines profiles.

We provide the first measurements of electric quadrupole hyperfine coupling constants for any atomic transition in any astrophysical object. We discuss the spectroscopic importance of the quadrupole terms. The inclusion of the quadrupole terms improves the measurement of the magnetic dipole constants, which are otherwise affected by a statistical bias.

As an application we have set a 3σ upper limit on the aluminium isotopic ratio, $^{26}\mathrm{Al}/^{27}\mathrm{Al} < 1/33$. This is the most stringent upper limit on the relative ^{26}Al abundance in any astrophysical object to date.

However, the accuracy of our measurement is short of quantifying ^{26}Al production in AGB stars. The expected isotopic ratio at the tip of the AGB is at most 1/37, from the ratio of the ^{26}Al and ^{27}Al yields in the 6 $M_\odot$ models of Forestini & Charbonnel (1997). The progenitor mass of NGC 6302 is about 5–6 $M_\odot$ from the data summarized in Casassus et al. (2000), but the predicted $^{26}\mathrm{Al}/^{27}\mathrm{Al}$ ratio lies below our 3σ upper limit. We can only discard $R_{\rm iso} = 1/37$ at 2.5σ. Doubling our integration on [Al VI] in NGC 6302 would allow a firm test on the theoretical predictions.

To establish useful constraints on the ^{26}Al production by AGB stars, we must deepen our observations of NGC 6302, and extend the analysis to other targets. Only PNe and symbiotic stars have moderate expansion velocities and photoionized coronal line regions, offering narrow emission-line profiles in high-excitation species, which are otherwise thermally broadened in the Sun.

ACKNOWLEDGMENTS

Many thanks are due to the Gemini support team, in particular Tom Geballe, Bob Blum and Bernadette Rodgers. Thanks also go to Andrés Jordan for the PDL::MINUIT package. SC acknowledges support from Fondecyt grant 1030805, and from the Chilean Centre for Astrophysics FONDAP 15010003. The work reported herein is based on observations obtained at the Gemini Observatory, which is operated by the Association of Universities for Research in Astronomy, Inc., under a cooperative agreement with the NSF on behalf of the Gemini partnership: the National Science Foundation (USA), the Particle Physics and Astronomy Research Council (UK), the National Research Council (Canada), CONICYT (Chile), the Australian Research Council (Australia), CNPq (Brazil) and CONICET (Argentina).

REFERENCES

Abt A., 1952, ApJ, 115, 199
Ashley M. C. B., Hyland A. R., 1988, ApJ, 331, 532
Banerjee D. P. K., Ashok N. M., Launila O., Davis C. J., Varricatt W. P., 2004, ApJ, 610, L29
Barlow M. J., Crawford I. A., Diego F., Dryburgh M., Fish A. C., Howard I. D., Spyromilio J., Walker D. D., 1995, MNRAS, 272, 333
Booth A. J., Blackwell D. E., 1983, MNRAS, 204, 777
Boreiko R. T., Betz A. L., Zmuidzinas J., 1988, ApJ, 325, L47
Brink D. M., Satchler G. R., 1994, Angular Momentum. Oxford Univ. Press, Oxford
Casassus S., Roche P. F., Barlow M. J., 2000, MNRAS, 314, 657

CERN, 1998, Program Library entry DS506, MINUIT – Function Minimization and Error Analysis
Charbonneau P., 1995, ApJS, 101, 309
Clayton D. D., 1994, Nat, 368, 222
Clegg R. E. S., Storey P. J., Walsh J. R., Neale L., 1997, MNRAS, 284, 348
Cooper T. G., Billowes J., Campbell P., Pearson M. R., 1996, J. Phys. G, 22, 99
De Natale P., Bellini M., Goetz W., Prevedelli M., Inguscio M., 1993, Phys. Rev. A, 48, 5
Diehl R. et al., 1995, A&A, 298, 445
Eissner W., Jones M., Nussbaumer H., 1974, Comput. Phys. Commun., 8, 270
Forestini M., Charbonnel C., 1997, A&AS, 123, 241
Forestini M., Arnould M., Paulus G., 1991, A&A, 252, 597
Glass R., Hibbert A., 1978, J. Phys. B, 11, 2257
Gomez Y., Moran J., Rodriguez L. F., Garay G., 1989, ApJ, 345, 862
Hinkle K. H. et al., 2003, Proc. SPIE, 4834, 353
Kelly D. M., Lacy J. H., 1995, ApJ, 454, L161
Meaburn J., Walsh J. R., 1980, MNRAS, 191, 5
Meléndez J., 1999, MNRAS, 307, 197
Prantzos N., 2004, MNRAS, 420, 1033
Press H. W., Teukolsky S. A., Vetterling W. T., Flannery B. P., 1986, Numerical Recipes. Cambridge Univ. Press, Cambridge
Raghavan P., 1989, Astrophys. Data Nucl. Data Tables, 42, 189
Rothman L. S. et al., 1992, J. Quant. Spectrosc. Radiat. Transfer, 48, 469
Townes C. H., Schawlow A. L., 1955, Microwave Spectroscopy. McGraw-Hill, New York
Turner B. E., Gammon R. H., 1975, ApJ, 198, 71
Wayte R. C., Wynne-Jones I., Blades J. C., 1978, MNRAS, 182, 5P
Winkler C. et al., 2003, A&A, 411, L1
Ziurys L. M., Apponi A. J., Yoder J. T., 1992, ApJ, 397, 123

This paper has been typeset from a TEX/LATEX file prepared by the author.